PHILOSOPHICAL TRANSACTIONS A

royalsocietypublishing.org/journal/rsta

Review

Cite this article: Arrieta J, Jeanneret R, Roig P, Tuval I. 2020 On the fate of sinking diatoms: the transport of active buoyancy-regulating cells in the ocean. *Phil. Trans. R. Soc. A* **378**: 20190529.
http://dx.doi.org/10.1098/rsta.2019.0529

Accepted: 2 April 2020

One contribution of 13 to a theme issue 'Stokes at 200 (part 2)'.

Subject Areas:
oceanography, cellular biophysics, fluid mechanics

Keywords:
phytoplankton, microscale, mechanosensing

Author for correspondence:
I. Tuval
e-mail: ituval@imedea.uib-csic.es

THE ROYAL SOCIETY PUBLISHING

On the fate of sinking diatoms: the transport of active buoyancy-regulating cells in the ocean

J. Arrieta[1], R. Jeanneret[2], P. Roig[1] and I. Tuval[1,3]

[1]Instituto Mediterráneo de Estudios Avanzados, IMEDEA, UIB-CSIC, 07190 Esporles, Spain
[2]Laboratoire de Physique de l'Ecole normale supérieure, ENS, Université PSL, CNRS, Sorbonne Université, Université de Paris, F-75005 Paris, France
[3]Departamento de Física, Universitat de les Illes Balears, 07122 Palma de Mallorca, Spain

JA, 0000-0003-1260-6168; RJ, 0000-0002-9444-9129; IT, 0000-0002-6629-0851

Diatoms are one of the most abundant, diverse and ecologically relevant phytoplanktonic group, contributing enormously to global biogeochemical processes like the carbon and silica cycles. This large success has been partly attributed to the mechanical and optical properties of the silica shell (the frustule) that envelops their body. But since they lack motility it is difficult to conceive how they cope with the fast-fluctuating environment they live in and where distributions of resources are very heterogeneous and dynamical. This pinpoints an important but yet poorly understood feature of diatoms physiology: buoyancy regulation that helps them controlling their sinking speed and position in the water column. While buoyancy regulation by light and nutrients availability has been well studied, the effect of hydromechanical stress via fluid shear has been rather overlooked when considering diatoms dynamics. Here, we aim to start filling this gap by first presenting direct experimental evidences for buoyancy control in response to hydro-mechanical stress and then review recent theoretical models where simple couplings between local shear and buoyancy control always result in heterogeneous cell distributions, specific accumulation regions within complex flows and increased sedimentation times to the depths, features of direct ecological relevance. We conclude by suggesting future experiments aiming

to unveil such coupling and therefore gain better understanding on the fate of these fascinating microorganisms in their natural habitat.

This article is part of the theme issue 'Stokes at 200 (part 2)'.

1. Introduction

Diatoms are non-motile unicellular photosynthetic eukaryotes constituting one of the most abundant and species-rich phytoplanktonic groups. With over 200 genera identified and more than 100 000 extant species estimated, diatoms show a large variety of morphologies, sizes (from approx. 1 µm to 100 µm) and life styles, existing either as isolated single cells or as chains of interconnected individuals [1]. Their most evident taxonomic characteristic is the presence of a specialized cell wall, known as the frustule, that is in large part made up of silica [2]. This cell wall consists of two intricately sculpted units, the valves, that are linked together through a structure called the girdle, enclosing the cell as within a closed Petri dish. The ability of diatoms to produce beautiful micro- and nano-structures through silica biogenesis has received great attention recently for its potential application in nanotechnology [3,4] and photonics [5,6]. Moreover, diatoms are essential for global-scale biogeochemical cycles [7–10] (including carbon [11,12] and silica [13]), greatly influencing the functioning of the whole marine ecosystem [7]. For instance, it is estimated that diatoms produce by photosynthesis as much organic carbon as half the terrestrial rainforests combined [11,14]. But as opposed to plants, this organic carbon is rapidly consumed, serving as the base for the marine food-web, supporting fisheries in coastal waters and the flourishing of micro-organisms at depth [15]. Moreover, their sedimentation transports approximately 6.3 Tmol of silica per year to the deep ocean [13]. In fact, global ocean fluxes of organic matter are partly controlled by this coupling between the sinking of decaying phytoplankton blooms and aggregates [16–18] and other biophysical processes (such as particle coagulation [16] and diatom–bacteria interactions in the so-called phycosphere [19–22]).

Because they prevalently lack motility (gliding has been observed only in some benthic species [23–25]), the dynamics of diatoms is influenced by two factors, advection by fluid flows and sinking due to density mismatch with seawater. But contrary to long-time beliefs, these micro-organisms are not solely passive particles. Indeed, they have developed the ability to actively regulate their buoyancy (and therefore their sinking speed) in response to environmental cues, notably light and nutrient availability [26,27]. This regulation inevitably impacts the sinking dynamics of diatoms and, as a consequence, has the potential to significantly affect the fate of diatom blooms, their reproductive strategies [28], the vertical transport of organic matter and, eventually, the biological carbon pump. Since diatoms mainly thrive under turbulent environments [29], it also appears natural to question the role of hydro-mechanical stimulus on this buoyancy regulation. However, in spite of first evidence showing active responses to fluid shear [26], almost no studies have been dedicated to shed light on the potential coupling between external mechanical stimulus and sinking dynamics.

In this article, we aim to emphasize the role that such coupling can have on diatoms' patchiness, community segregation and sedimentation times to the depths. To that purpose, we first briefly discuss the different means by which diatoms are known to alter their buoyancy, as well as preliminary laboratory experiments that demonstrate this coupling between mechano-sensing and buoyancy control does exist. We then present the highly relevant results obtained in theoretical studies that consider simple mathematical forms for this coupling.

2. Mechanosensing and buoyancy control

How do diatoms sink in the water column? For a small ($\sim$ micro/millimetric) spherical particle of uniform density ρ_p sinking under quiescent conditions, fluid inertia is negligible (low Reynolds number limit) and the particle speed can be determined by a balance between buoyancy and

viscous forces, leading to the well-known Stokes' Law

$$V_s = \frac{2(\rho_p - \rho_F)ga^2}{9\mu}, \tag{2.1}$$

where a is the particle radius, g Earth gravity, ρ_F the fluid density and μ its dynamic viscosity. This law exhibits a quadratic dependence of sinking speed with particle size (dashed yellow (light) line in figure 1*a*) which does not accurately account for the experimentally measured sinking speeds of living and dead diatoms (dots in figure 1*a*). A slightly more appropriate approximation consists in fact in taking into account the difference in volume and density between the heavy (but thin) silicate frustule and the light (but large) cytoplasm [31], which leads to the following modified Stokes' Law:

$$V_s = \frac{2g}{9\mu}\left[\rho_{\mathrm{cyt}}\frac{(a-t)^3}{a} + \rho_{\mathrm{fr}}\frac{3a^2t - 3at^2 + t^3}{a} - \rho_F a^2\right], \tag{2.2}$$

where ρ_{cyt} and ρ_{fr} are the densities of the cytoplasm and the frustule, respectively, and t the thickness of the silica shell. If we consider t to be independent of the cell size a, this modified law matches relatively well the measurements performed by C. S. Reynolds with dead *Stephanodiscus rotula* cells (black (dark) dots). However, living cells of the same species (green light squares) deviate considerably, presenting significantly slower sinking speeds than those expected for their size. In fact, the variability of compiled diatoms' sinking speeds (obtained from many species in different physiological states [31]) is so huge (blue light dots), that we cannot reasonably consider such a simple law to hold universally. Beyond geometrical effect (on viscous forces) due to the diversity of cell shapes, this variability suggests active buoyancy regulation by the cells depending on their physiological states [32], and therefore on the environment (light [33], nutrients [34]) they are confronted with.

In fact, it has been shown that diatoms have evolved different means by which to regulate their density. They do so at a metabolic cost by bio-silicification [35], active replacement of heavy ions by light ions in the vacuole [36–38] (that in some cases occupies up to 90% of the cytoplasm) or carbohydrate reduction [39,40]. These diverse mechanisms take place over distinct time scales: while an increase in cell silicification occurs in periods of several hours to days, and carbohydrates accumulate and act as ballasts in a few minutes, ion replacement occurs in even shorter time scales. In their seminal work, Falciatore *et al*. [26] showed for the first time how diatoms are capable of responding actively to environmental (e.g. light, nutrient or osmotic) stress. Using *Phaeodactylum tricornutum* as a model diatom, these active responses were measured by the transient production of cytosolic Ca^{2+}, which is a characteristic proxy for the activation of many signal transduction pathways [41]. Remarkably, cytosolic calcium transient release was also observed when diatoms were exposed to mechanical stimuli [26,27]. Cells detect and respond to fluid motion (shear stress) by a fast (1–2 s) production of cytosolic Ca^{2+} followed by a slower decay of the intracellular concentration in tens of seconds. This response is also adaptive, with a recalcitrance period of the order of minutes. More recent results have also shown that diatoms exposed during long periods (approx. 48 h) to turbulent flows, modify their metabolic pathways increasing the biosynthesis of fatty acids and their lipid metabolism [42] which, in turn, inevitably alter cell density.

Motivated by the results presented above, we have performed a series of novel preliminary experiments designed to quantify the effect of fluid shear on buoyancy regulation on short time scales. A suspension of *Thalassiosira pseudonana*, approximately 10 µm in size, cultured in a diurnal chamber under standard laboratory conditions (in Guillard's f/2-medium + silica (15 mg l^{-1}), 16:8 light/dark cycle at 20°C) was loaded into a vertically oriented PDMS channel (5 cm long and 1.4 × 1.4 mm in cross section) through which a periodic 'on/off' flow (of period $T = 10$ s, flow vertically upwards) was imposed by an external syringe pump (fusion 200; Chemyx). The applied shear rates ∼0.1–1 s^{-1} (applied flow-rate $q \in [10, 100]$ µl min^{-1}) provided by this set-up to the cells are compatible with those commonly experienced in coastal and oceanic settings. Individual cells were observed through a continuously focusable video-microscope (Infinivar GS; Infinity)

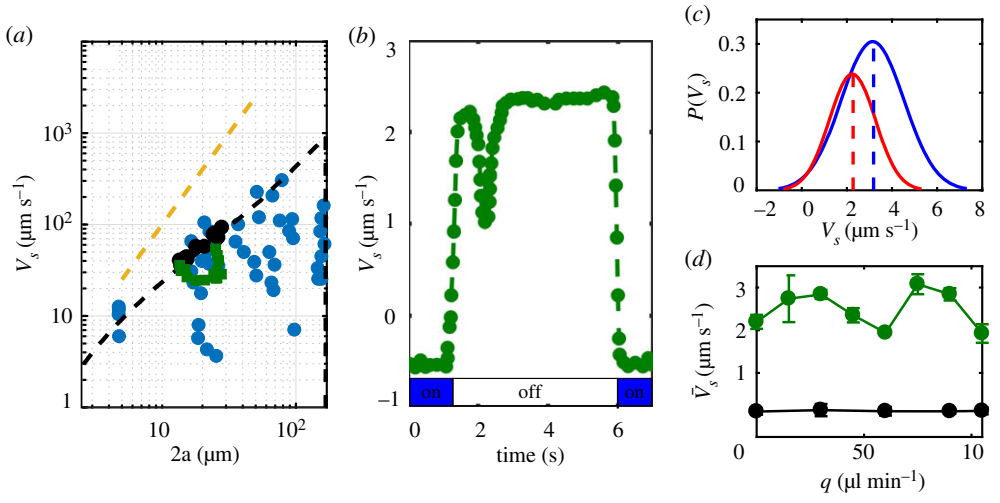

Figure 1. (*a*) Mean sinking speed of diatoms as a function of their cell diameter: adapted with permission from [30] for *Stepahnodiscus rotula* for both living (solid green (light) squares) and dead cells (black (dark) circles) and for many other species in a variety of physiological states as compiled by Miklasz & Denny [31] (blue (light) circles). Yellow (light) line shows Stokes' Law for spherical particles of uniform density and that presents a quadratic dependence on a (2.1) for $\rho_p = 1800$ kg m^{-3}; the dashed black (dark) line instead shows a modified Stokes' Law (2.2), for particles with an inhomogeneous density distribution with $t = 1\,\mu$m, $\rho_{cyt} = 1065$ kg m^{-3} and $\rho_{fr} = 1800$ kg m^{-3}. (*b–d*) New experimental data showing effect of shear stresses in modifying the sinking speed of diatoms. (*b*) The instantaneous sinking speed of a representative experiment: cells were exposed to a binary 'on/off' cycle of applied constant flow rate $q = 50\,\mu$l min^{-1} and with a period of 10 s. During 'on' periods cells are dragged along with the flow at a constant speed ($\sim 3\,\mu$m s^{-1}). During 'off' periods cells show a significant response after the mechanical stimulus have decayed with a rapid burst (decrease) in sinking speed. (*c*) The distribution of instantaneous sinking speeds varies with forcing amplitude (i.e. flow rate): solid red line (light) represents the distribution of sinking speed without mechanical stimulus ($q = 0\,\mu$l min^{-1}) while blue (dark) solid line shows $P(V_s)$ for the same cells after 10 periods of forcing with $q = 75\,\mu$l min^{-1}. (*d*) The mean sinking speed, $\bar{V}_s$, depends nonlinearly on forcing amplitude: results for physiologically active cells are shown in green (light); black (dark) dots represent dead cells. Errorbars: standard deviation of the measurement set for each flow rate. (Online version in colour.)

at high magnification (*ca* x10) at high enough temporal resolution (with an UI-3370CP-NIR-GL R2 camera; IDS) to allow accurate determination of their instantaneous sinking speed (during the 'off' flow phases) via particle tracking [43].

As illustrated by the evolution of the instantaneous cell speed in a representative experiment (figure 1*b*), soon after the flow is stopped, cells exhibit a clear response with a rapid (approx. 50%) drop in sinking speed during the 'off' period. Interestingly, the time scale of this rapid change in sinking speed (approx. 1–2 s) compares with those observed for the calcium spikes in [26]. An experimental sweep in the applied flow rates also shows that the distribution of instantaneous sinking speeds significantly varies with forcing amplitude with approximately 50% change in the mean sinking speed, $\bar{V}_s$, for physiologically active cells in the explored range of shear rates (figure 1*b*,*c*). Control runs with dead cells represented by black (dark) dots in figure 1*d* (slowed down by increasing the viscosity of the fluid with 0.5% methylcellulose to facilitate the tracking of the cells) showed no equivalent variation. Therefore, these preliminary results strongly suggest that diatoms mechano-sensing capability yields fast active physiological responses determining instantaneous cell density. Although further experimental work is needed to really disentangle the relationship between hydro-mechanical stress and buoyancy control and, in particular, to decipher the physiological pathways between the active replacement of ions in the vacuole and the production of intracellular Ca^{2+}, we will demonstrate in the following section the importance of such coupling on the large-scale properties of cell communities in complex flows.

3. Transport and spatial distribution of non-motile buoyancy regulating phytoplankton

Phytoplankton live in a turbulent environment [44,45] where resources are patchy and scarce. Hence, oceanic and coastal flows shape the spatial distribution of phytoplankton. This spatial heterogeneity affects essential ecological interactions, including population stability [46], species diversity or predator–prey dynamics [47], which are relevant for the functioning of the whole marine food web [48]. Patchiness has different origins at different scales. While at the mesoscale it is mainly dominated by reproduction, grazing, nutrient availability [49] and large-scale advection [50], at smaller scales (i.e. $\lesssim$1 m) the interplay between environmental stresses and cell physiological responses becomes more relevant.

The interaction of motile phytoplankton with surrounding flows has been intensively studied and is known to regulate encounter rates [51,52], to affect the formation of thin layers [53] or to induce cell clustering [54] and segregation [29]. On the other hand, our current understanding of the microscopic processes responsible for patchiness in non-motile marine micro-organisms is much more limited. Motivated by the evidence of buoyancy control in diatoms and their ability to perceive mechanical stress (as detailed in §2), recent theoretical studies have started to explore the role of the interplay between buoyancy regulation and advection on large scale properties of cell communities [55,56]. Here, we review the most relevant findings obtained from these models.

(a) Theoretical approach

The motion of a small spherical particle embedded in a background fluid flow is well described by the Maxey–Riley equation [57,58]. Its non-dimensional form can be obtained using the characteristic length L_c, time t_c and velocity u_c of the background flow:

$$(1-R/2)\rho_p\frac{d^2\mathbf{x_p}}{dt^2}=[(1-R/2)\rho_p-R]\frac{v_s}{(1-3R/2)\mathrm{St}}\mathbf{k}+R\frac{D\mathbf{u}}{Dt}-\frac{R}{2}\frac{d}{dt}(\mathbf{u}_p-\mathbf{u})+\frac{1}{St}(\mathbf{u}-\mathbf{u}_p), \quad (3.1)$$

where $\mathbf{x}_p$ is the position of the particle, $\mathbf{u}_p$ its velocity, $\mathbf{k}$ a unit vector along the gravity direction, $\mathbf{u}$ the fluid velocity, D/Dt the derivative along the path of a fluid element, d/dt the derivative along the trajectory of the particle, $\mathrm{St}=2a^2/(9\nu Rt_c)$ the Stokes number ($\nu=\mu/\rho_F$ is the fluid kinematic viscosity), $R=\rho_F/(\rho_0+\rho_F/2)$ the mass ratio (with ρ_0 the maximum density of the particle, see below) and $v_s=2a^2gt_c(1-3R/2)/(9\nu RL_c)$ the maximum non-dimensional (still fluid) sedimentation velocity of the particle. Within this framework we will consider two distinct cases: (i) the Taylor–Green vortex (TGV) flow [59,60], a two-dimensional (2D) laminar steady flow which is an exact analytical solution of the Navier–Stokes equations. In this case, L_c can be naturally chosen as the characteristic vortex length, t_c the inverse of the vorticity at the centre of the vortex, and $u_c=L_c/t_c$. (ii) A three-dimensional (3D) fully turbulent isotropic flow, where the characteristic quantities are naturally given by the involved Kolmogorov scales [61]. The former 2D case, used in [55], provides an explicit analytical expression for the velocity field, while the later, presented in [56], requires the numerical integration of the 3D Navier–Stokes equations with a zero-mean, temporally uncorrelated Gaussian forcing term in the momentum equation, that injects energy at large scales at a given rate, ϵ, to sustain a statistically steady state.

The particle motion is dictated by three non-dimensional parameters: the Stokes number St, the mass ratio R and the sedimentation velocity of the particle v_s. If the particle Stokes number is small and derivatives following the particle are well approximated by derivatives following the fluid (i.e. $\mathrm{d}/\mathrm{d}t\simeq D/Dt$), then the equation of motion reduces to [56]

$$\frac{\mathrm{d}\mathbf{x_p}}{\mathrm{d}t}=\mathbf{u}-v_s'\mathbf{k}, \quad (3.2)$$

where $v_s'=a^2gt_c(1-\beta')/(3\nu\beta'L_c)$ is the instantaneous sinking velocity with $\beta'=3\rho_F/(2\rho_p+\rho_F)$.

The originality of the model consists in complementing this momentum conservation equation with a coupling term between ρ_p, the particle density, and the norm of the local strain tensor $\dot{\varepsilon}$.

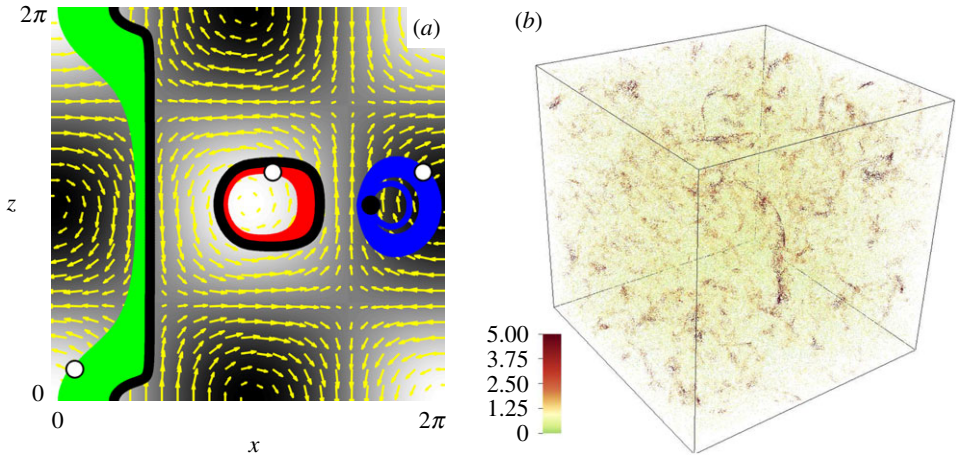

Figure 2. Representative trajectories for active buoyancy regulating particles obtained by the numerical integration of (3.1) in the 2D TGV flow for the passive case (green (light grey) line), the shear-thinning case (blue (dark grey) line) and the shear-thickening case (red (medium grey) line) (*a*). The 3D turbulent case, obtained by the integration of (3.2) (*b*), shows clustering of particles when looking at their spatial distributions. This is illustrated by plotting the ratio of the local number density of particles to the average number density. Figures adapted with permission from [55,56]. (Online version in colour.)

We consider two situations for this coupling, with particles either decreasing or increasing their density with $\dot{\varepsilon}$ (which, in an analogy to standard rheology but referring to the behaviour of the particles' density instead of the behaviour of fluids with varying strain rate, we dubbed *shear-thinning* and *shear-thickening* particles, respectively). As the detailed mechanism responsible for how intracellular responses translate into the regulation of buoyancy is still unclear, we make ρ_p vary between ρ_F (neutral buoyancy) and $\rho_0 = 2\rho_F$ with a linear dependency with the response function $f(\dot{\varepsilon})$. Finally, this response function has been given either a linear dependency on $\dot{\varepsilon}$ or a probably more realistic Michaelis–Menten functional form $f(\dot{\varepsilon}) = \dot{\varepsilon}/(\dot{\varepsilon} + \dot{\varepsilon}_H)$ with $\dot{\varepsilon}_H$ a half-saturation constant.

Before presenting the specific results obtained with this model, it should be noted that we have implicitly assumed a number of approximations in what precedes. First, for simplicity and following many [58,62,63], we have neglected the Faxén correction and Basset history terms in the original Maxey–Riley equation (equation (3.1)). Second, the final equation for particle motion (equation (3.2)) neglects inertia, which constitutes a natural approximation given the small values of the Stokes number encountered in typical turbulent flows [56]. Last, we consider particles that regulate their buoyancy instantaneously, in reasonable agreement with the rapid nature of the response discussed above. However, this neglects particle history effects expected from the potential adaptive nature of the active response of the cells [26]. Of course, relaxing these different approximations would constitute interesting extensions, the impact of which is worth dedicated future research.

(b) Clustering and patchiness in the distribution of particles

We have integrated numerically (3.1) (or (3.2)) together with $f(\dot{\varepsilon})$ with particles initially distributed uniformly within the 2D or 3D spatial domain. The final distribution of the particles' position was obtained after sufficiently large integration times to asses statistically significant steady-state results. Active buoyancy regulation has a first striking effect on the sinking dynamics for all explored cases: it enhances the clustering of particles.

This is clearly shown in figure 2. Within the 2D steady TGV flow, while passive particles sink indefinitely for any inertial perturbation [64–66] (green (light grey) track in figure 2*a*), clustering of active particles (red (medium grey) track: shear-thickening; blue (dark grey) track: shear-thinning)

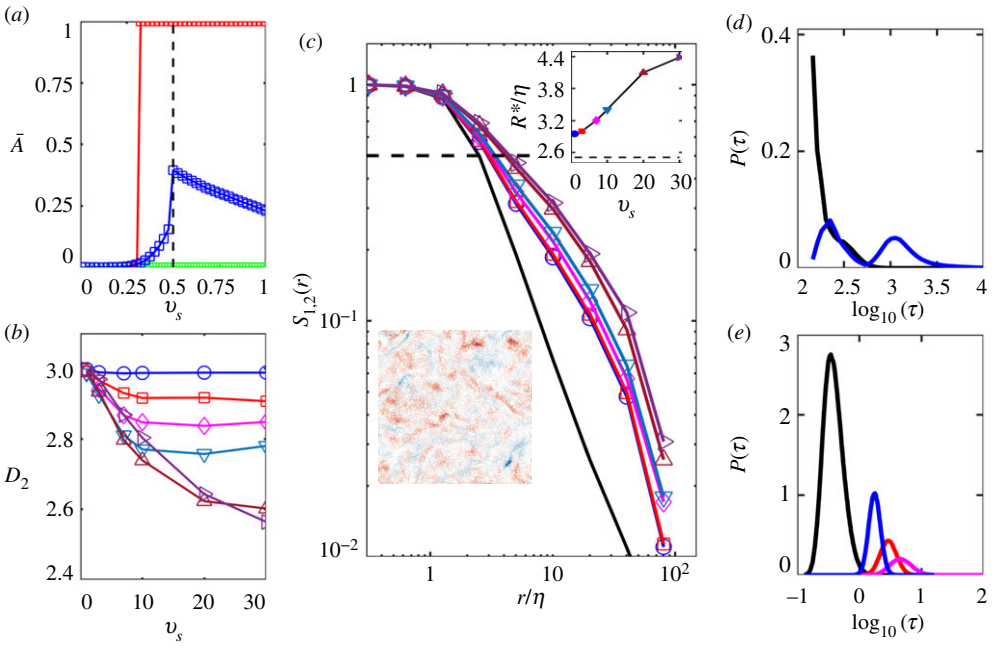

Figure 3. Patchiness is quantified by (*a*) the area of attraction $\bar{A}$ for the passive case (green (light grey)), the shear-thinning case (blue (dark grey)) and the shear-thickening case (red (medium grey)) and (*b*) the correlation dimension D_2 for shear-thickening particles and different values of $\dot{\varepsilon}_H$ denoted by different colours. Both cases display a marked functional dependence with the still fluid sedimentation velocity, v_s. (*c*) This is also true for the segregation of populations with distinct levels of activity as clearly seen in a 2D section of the 3D integration box. Distributions of escape times $P(\tau)$ for (*d*) passive (black (dark) solid line) and shear-thinning (blue (light) line) particles in the TGV flow and (*e*) for active particles in 3D isotropic turbulence and different values of $\dot{\varepsilon}_H$. Figures adapted with permission from [55,56]. (Online version in colour.)

occurs by their trapping in attractive invariant structures (fixed points and limit cycles) of the underlying dynamics. Within a 3D isotropic turbulent flow such invariant structures do not exist. Nevertheless, while passive particles are solely rearranged uniformly within the domain (not shown), buoyancy regulating particles display a large degree of clustering as illustrated by the snapshot of local number density (of shear-thinning particles) in the domain, figure 2*b*. In order to quantify the degree of clustering, we use the area $\bar{A}$ of the basin of attraction of the attractors in the 2D TGV flow, while we make use of the correlation dimension D_2 of the steady distribution in 3D isotropic flow. This last quantity is defined as the scaling exponent of the probability of finding two particles at a distance less than $r : P(|\mathbf{x}_1 - \mathbf{x}_2| < r) \propto r^{D_2}$, as $r \to 0$. In a 3D domain, if $D_2 < 3$, the probability of having particles at small distances decays more slowly than for a homogeneous distribution, an indication of fractal clustering. In an ecological sense, D_2 is directly related to the encounter rate between cells. Figure 3*a*,*b* shows how the level of clustering strongly depends on the non-dimensional sinking speed v_s and other model parameters (e.g. $\dot{\varepsilon}_H$ in figure 3*b*). While for a laminar flow the maximum degree of trapping is achieved for $v_s \sim u_c$, for a turbulent flow the largest clustering correspond to larger values of v_s. With $\epsilon = 10^{-9}\,\mathrm{W\,kg^{-1}}$, which is of the order of the energy injection rate encountered in the open ocean, this corresponds to 0.18 mm s^{-1} and 5.4 mm s^{-1} still fluid sinking speeds, respectively.

(c) Community segregation

Another phenomenon of paramount importance in ecology, and which is closely related to patchiness, is community segregation. The degree of spatial overlap is a hallmark of biological diversity as it facilitates the competition for resources by allowing distinct populations to explore

different ecological niches. To understand how community segregation in non-motile species is affected by buoyancy regulation, we analyse the segregation between distinct populations within a common background flow. For instance, a shear-thickening and a shear-thinning population characterized by different values of $\dot{\varepsilon}_H$ and v_s do not explore the 3D space in a similar manner and can be therefore expected to segregate [56].

A classical measure of segregation is the index $S_{1,2}(r)$ introduced in [67], and defined by $S_{1,2}(r) = 1/(N_1 + N_2) \sum_i^{M(r)} |n_i^1 - n_i^2|$ where $M(r)$ is the number of cubes of side r in which the domain L^3 is partitioned, N_1, N_2 the total number of particle of each species, and n_i^1, n_i^2 the number of particles of each type in cube index i. This quantity is then defined in $[0, 1]$: $S_{1,2}(r) = 0$ implies that the total number of particles of the two types is the same at a given scale r, while the opposite limit, $S_{1,2}(r) = 1$, implies that there is no overlapping between the two spatial distributions and the populations are completely segregated at that scale. Complete separation is expected at very small scale, giving that $\lim_{r\to 0} S_{1,2}(r) = 1$, while no structure can be observed on the scale of the numerical box, with $\lim_{r\to L} S_{1,2}(r) = 0$. Finally, the segregation length scale R^* is defined as $S_{1,2}(R^*) = 1/2$ and constitutes a limit below which the two populations can be considered as not overlapping, and therefore segregated. To explore the effect of buoyancy control on the segregation of communities, we consider mix populations composed of shear-thinning cells (with fixed $\dot{\varepsilon}_H^{(\mathrm{thin})}$ and $v_s^{(\mathrm{thin})}$) and shear-thickening cells (with fixed $\dot{\varepsilon}_H^{(\mathrm{thick})}$ but varying $v_s^{(\mathrm{thick})} = v_s$). Figure 3*c* depicts the evolution of the segregation index in a homogeneously distributed suspension (i.e. passive particles, solid black line) and in the active system for the different values of v_s used (solid colour lines). Clearly, the segregation index remains close to 1 for larger r in the active cases, showing that different buoyancy control strategies between species naturally lead to community segregation. Such segregation is illustrated by the snapshot (bottom-left inset in figure 3*c*) of local number densities for the two populations (red (light): shear-thinning; blue (dark): shear-thickening). Although the correlation dimension D_2 of the fractal attractors for the two individual populations is almost identical under the chosen set of parameters (not shown), their dynamics are not necessarily overlapping, leading to well-segregated populations. Finally, the corresponding segregation length scale R^* increases monotonically with the normalized maximum sinking speed of the shear-thickening population v_s.

(d) Sinking to depth

Changes in the sinking speed due to buoyancy control affect the time it takes cells and aggregates to reach the deep ocean, an ecologically relevant process driving the biological carbon pump and fundamental for the estimate of downward fluxes of organic matter [68]. The results discussed in the previous sections imply that care should be taken when analysing the sinking dynamics of non-passive particles, as the interplay between advective contributions and physiological control translates into diverse forms. In order to investigate the effect of buoyancy regulation in the distribution of escape times to the deep ocean, we use as a proxy the time τ needed for particles to cover a large vertical distance, i.e. several times $n \gg 1$ the size L_B of the periodic integration box of our doubly (or triply) periodic domain. Buoyancy control notably increases τ for active particles when compared to the sinking of purely passively advected ones.

For TGV flow, even in the region of the parameter space where no permanent trapping exists [55], the distribution of time τ is bimodal in the case of buoyancy regulating cells, showing a highly heterogeneous escape dynamics, figure 3*d* blue (light) curve. This is in contrast with the distribution of τ for passive particles (with the same set of parameters), which exhibit a simple exponential decay with much smaller average escape time, figure 3*d* black (dark) curve. Similarly, for 3D isotropic turbulent flows the escape time τ displays increased mean values and much broader distributions (i.e. the probability density functions $P(\tau)$ display wider tails) as a function of cell activity (figure 3*e*). In other words, buoyancy regulation does not simply shift the distributions rigidly but also modifies its shape, i.e. a larger fraction of the population remains suspended for a time significantly larger than the average population. The major effect of buoyancy regulation in this respect is to reduce the time-averaged 'instantaneous cell density'

(and as a consequence the instantaneous sinking speed) well below the maximum passive value, effectively keeping cells suspended for much longer times before ultimately sinking to the deep ocean.

4. Conclusion

Diatoms are one of the most successful phytoplankton groups, whether in terms of their abundance, diversity or cosmopolitan nature. Diatoms contribute significantly to ocean primary productivity, forming a substantial basis of the marine food web and, as a result, partially determining the dynamics of the whole marine ecosystem. Moreover, diatoms have a fundamental impact on global climate through their major contribution to oxygen production, their role in the biological carbon pump and CO_2 sequestration and in other global biogeochemical oceanic cycles. Their rapid sinking to the deep ocean is greatly facilitated compared to other phytoplankton group due to their characteristic heavy silicate wall. However, it does not simply follow from Stokes' Law: diatoms have evolved sophisticated mechanisms to efficiently modify their density as an active response to environmental cues. This is physiologically achieved by means of bio-silicification, carbohydrate ballast or ion replacement in the vacuole; all processes with a substantial metabolic cost.

Our preliminary experimental results further establish that diatoms' buoyancy is not only regulated by light or availability of nutrients but that it is also controlled by hydro-mechanical stress. This strongly supports previous speculations that mechanically induced fast intracellular responses, in the form of cytosolic Ca^{2+} spikes [26], are involved in downstream mechanotransduction that translates into changes of cellular mass density. In fact, we have shown significant changes (up to 50%) in the sinking speed of *Thalassiosira pseudonanna* cells after these have been briefly exposed to shear level comparable to those naturally encountered in the sea. Although these reveal that diatoms are indeed able to modify buoyancy in response to external flows, further experiments are needed in order to fully elucidate this interplay and to eventually provide theoretical grounding for the observed active responses. Furthermore, we recall that we expect buoyancy control to become even more important for larger species of diatoms, such as *Coscinodiscus walesii*, for which the volume of the vacuole is larger, and larger variations in undisturbed sinking speeds have already been observed [33,34]. Most importantly, in their natural fluid environment diatoms are under the continuous effect of fluid mechanical stresses. There the interplay between active physiological responses and physical transport processes becomes particularly relevant as it can dynamically modify cell behaviour, advected trajectories and, ultimately, phytoplankton spatial distribution with its relevance for many ecological processes in the sea. Recent theoretical work [55,56] has explored how this interplay results in enhanced population patchiness, community segregation and escape times to the deep ocean.

The results summarized herein suggest a number of pressing future research directions. Chief among them are detailed characterization of the effect of fluid mechanical stress on buoyancy regulation, its effect on nutrient uptake by altering the nutrient-deplete boundary layer around sinking cells [34], its role in promoting collective phenomena such as the formation of thin phytoplankton layer which should be addressed both theoretically and experimentally, and the experimental realization of active responses in vortical flows that can be explored by, for instance, employing a similar configuration as the one described in [54]. Moreover, long-term adaptive dynamics has not been addressed so far, despite evidence showing that long exposure to turbulence produces changes in diatoms in the expression of relevant metabolic pathways [42] and, similarly in other phytoplankton groups (such as dinoflagellates) where it can even trigger morphological changes resulting in cells evading regions of strong turbulence [69].

Data accessibility. The data employed to generate the figures of [56] are available at https://github.com/mborgnino/data-buoyancy-regulating-phytoplankton, whereas data employed to generate the figures of [55] and in figure 1 of this manuscript are available at https://github.com/jarrietasanagustin/review_diatoms.

Authors' contributions. J.A. and I.T. led the writing of the manuscript. R.J. and P.R. performed experiments and analysed experimental data. J.A., R.J. and I.T. contributed equally to the final version of the manuscript.

Competing interests. The authors declare that they have no competing interests.

Funding. We acknowledge the support from the Spanish Ministry of Economy and Competitiveness (AEI, FEDER EU) grant nos FIS2016-77692-C2-1-P (I.T. and J.A.) and CTM-2017-83774-D (J.A.). J.A thanks the Govern de les Illes Balears for financial support through the Vicenç Mut subprogram partially funded by the European Social Fund.

Acknowledgements. We acknowledge the fruitful collaboration with M. Borgnino, F. De Lillo and G. Boffetta from Università di Torino with whom part of the results discussed in this review were developed.

References

1. Kooistra WH, Gersonde R, Medlin LK, Mann DG. 2007 Chapter 11 - the origin and evolution of the diatoms: their adaptation to a planktonic existence. In *Evolution of primary producers in the sea* (ed. PG Falkowski, AH Knoll), pp. 207 – 249. Burlington, MA: Academic Press.
2. Round F, Crawford R, Mann D, Press CU. 1990 *Diatoms: biology and morphology of the genera*. Cambridge, UK: Cambridge University Press.
3. Kröger N, Poulsen N. 2008 Diatoms - from cell wall biogenesis to nanotechnology. *Annu. Rev. Genet.* **42**, 83–107. (doi:10.1146/annurev.genet.41.110306.130109)
4. Lopez PJ, Desclés J, Allen AE, Bowler C. 2005 Prospects in diatom research. *Curr. Opin. Biotechnol.* **16**, 180–186. (doi:10.1016/j.copbio.2005.02.002)
5. Fuhrmann T, Landwehr S, El Rharbi-Kucki M, Sumper M. 2004 Diatoms as living photonic crystals. *Appl. Phys. B* **78**, 257–260. (doi:10.1007/s00340-004-1419-4)
6. Stefano LD, Rotiroti L, Stefano MD, Lamberti A, Lettieri S, Setaro A, Maddalena P. 2009 Marine diatoms as optical biosensors. *Biosens. Bioelectron.* **24**, 1580–1584. (doi:10.1016/j.bios.2008.08.016)
7. Armbrust EV. 2009 The life of diatoms in the world's oceans. *Nature* **459**, 185–192. (doi:10.1038/nature08057)
8. Malviya S *et al.* 2016 Insights into global diatom distribution and diversity in the world's ocean. *Proc. Natl Acad. Sci. USA* **113**, E1516–E1525. (doi:10.1073/pnas.1509523113)
9. Zehr JP. 2010 Nitrogen fixation by marine cyanobacteria. *Trends Microbiol.* **19**, 162–173. (doi:10.1016/j.tim.2010.12.004)
10. Berman-Frank I, Lundgren P, Falkowski P. 2003 Nitrogen fixation and photosynthetic oxygen evolution in cyanobacteria. *Res. Microbiol.* **154**, 157–164. (doi:10.1016/S0923-2508(03)00029-9)
11. Field CB, Behrenfeld MJ, Randerson JT, Falkowski P. 1998 Primary production of the biosphere: integrating terrestrial and oceanic components. *Science* **281**, 237–240. (doi:10.1126/science.281.5374.237)
12. Richardson TL, Jackson GA. 2007 Small phytoplankton and carbon export from the surface ocean. *Science* **315**, 838–840. (doi:10.1126/science.1133471)
13. Tréguer PJ, De La Rocha CL. 2013 The world ocean silica cycle. *Annu. Rev. Mar. Sci.* **5**, 477–501. (doi:10.1146/annurev-marine-121211-172346)
14. Nelson DM, Tréguer P, Brzezinski MA, Leynaert A, Quéguiner B. 1995 Production and dissolution of biogenic silica in the ocean: revised global estimates, comparison with regional data and relationship to biogenic sedimentation. *Global Biogeochem. Cycles* **9**, 359–372. (doi:10.1029/95GB01070)
15. Sarthou G, Timmermans KR, Blain S, Tréguer P. 2005 Growth physiology and fate of diatoms in the ocean: a review. *J. Sea Res.* **53**, 25–42. (doi:10.1016/j.seares.2004.01.007)
16. Jackson GA. 1990 A model of the formation of marine algal flocs by physical coagulation processes. *Deep Sea Res. Part A. Oceanographic Res. Papers* **37**, 1197–1211. (doi:10.1016/0198-0149(90)90038-W)
17. Jackson GA, Kiørboe T. 2008 Maximum phytoplankton concentrations in the sea. *Limnol. Oceanogr.* **53**, 395–399. (doi:10.4319/lo.2008.53.1.0395)
18. Ragueneau O *et al.* 2000 A review of the Si cycle in the modern ocean: recent progress and missing gaps in the application of biogenic opal as a paleoproductivity proxy. *Global Planetary Change* **26**, 317–-365. (doi:10.1016/S0921-8181(00)00052-7)
19. Smriga S, Fernandez VI, Mitchell JG, Stocker R. 2016 Chemotaxis toward phytoplankton drives organic matter partitioning among marine bacteria. *Proc. Natl Acad. Sci. USA* **113**, 1576–1581. (doi:10.1073/pnas.1512307113)

20. Amin SA, Parker MS, Armbrust EV. 2012 Interactions between diatoms and bacteria. *Microbiol. Mol. Biol. Rev.* **76**, 667–684. (doi:10.1128/MMBR.00007-12)
21. Seymour JR, Amin SA, Raina JB, Stocker R. 2017 Zooming in on the phycosphere: the ecological interface for phytoplankton-bacteria relationships. *Nat. Microbiol.* **2**, 17065. (doi:10.1038/nmicrobiol.2017.65)
22. Azam F, Malfatti F. 2007 Microbial structuring of marine ecosystems. *Nat. Rev. Microbiol.* **5**, 782–791. (doi:10.1038/nrmicro1747)
23. Poulsen NC, Spector I, Spurck TP, Schultz TF, Wetherbee R. 1999 Diatom gliding is the result of an actin-myosin motility system. *Cell Motility* **44**, 23–33. (doi:10.1002/(SICI)1097-0169(199909)44:1<23::AID-CM2>3.0.CO;2-D)
24. Gessey G, Wigglesworth-Cooksey B, Cooksey K. 2000 Influence of calcium and other cations on surface adhesion of bacteria and diatoms: a review. *Biofouling* **15**, 195–205. (doi:10.1080/08927010009386310)
25. Bondoc K, Heuschele J, Gillard J, Vyverman W, Pohnert G. 2016 Selective silicate-directed motility in diatoms. *Nat. Commun.* **7**, 10540. (doi:10.1038/ncomms10540)
26. Falciatore A, Croot P, Bowler C. 2000 Perception of environmental signals by a marine diatom. *Science* **288**, 2363–2366. (doi:10.1126/science.288.5475.2363)
27. Falciatore A, Bowler C. 2002 Revealing the molecular secrets of marine diatoms. *Annu. Rev. Plant Biol.* **53**, 109–130. (doi:10.1146/annurev.arplant.53.091701.153921)
28. Font-Muñoz JS, Jeanneret R, Arrieta J, Anglès S, Jordi A, Tuval I, Basterretxea G. 2019 Collective sinking promotes selective cell pairing in planktonic pennate diatoms. *Proc. Natl Acad. Sci. USA* **116**, 15 997–16 002. (doi:10.1073/pnas.1904837116)
29. Margalef R. 1978 Life-forms of phytoplankton as survival alternatives in an unstable environment. *Oceanolog. Acta* **1**, 493–509.
30. Reynolds CS 2006 *The ecology of phytoplankton*. Ecology, biodiversity and conservation. Cambridge, UK: Cambridge University Press.
31. Miklasz KA, Denny MW. 2010 Diatom sinkings speeds: improved predictions and insight from a modified Stokes' law. *Limnol. Oceanogr.* **55**, 2513–2525. (doi:10.4319/lo.2010.55.6.2513)
32. Waite AM. 1992 *Physiological control of diatom sedimentation*. PhD thesis, University of British Columbia, Canada.
33. Du Clos KT, Karp-Boss L, Villareal TA, Gemmell BJ. 2019 *Coscinodiscus wailesii* mutes unsteady sinking in dark conditions. *Biol. Lett.* **15**, 20180816. (doi:10.1098/rsbl.2018.0816)
34. Gemmell BJ, Oh G, Buskey EJ, Villareal TA. 2016 Dynamic sinking behaviour in marine phytoplankton: rapid changes in buoyancy may aid in nutrient uptake. *Proc. R. Soc. B* **283**, 20161126. (doi:10.1098/rspb.2016.1126)
35. Raven JA, Waite AM. 2004 The evolution of silicification in diatoms: inescapable sinking and sinking as escape? *New Phytol.* **162**, 45–61. (doi:10.1111/j.1469-8137.2004.01022.x)
36. Gross F, Zeuthen E, Yonge M. 1948 The buoyancy of plankton diatoms: a problem of cell physiology. *Proc. R. Soc. Lond. B* **135**, 382–389. (doi:10.1098/rspb.1948.0017)
37. Anderson LWJ, Sweeney BM. 1978 Role of inorganic ions in controlling sedimentation rate of a marine centric diatom *Ditylum brightwelli*. *J. Phycol.* **14**, 204–214. (doi:10.1111/j.1529-8817.1978.tb02450.x)
38. Boyd C, Gradmann D. 2002 Impact of osmolytes on buoyancy of marine phytoplankton. *Mar. Biol.* **141**, 605–618. (doi:10.1007/s00227-002-0872-z)
39. Richardson T, Cullen J. 1995 Changes in buoyancy and chemical composition during growth of a coastal marine diatom: ecological and biogeochemical consequences. *Marine Ecol. Progress Ser.* **128**, 77–90. (doi:10.3354/meps128077)
40. Fisher AE, Harrison PJ. 1996 Does carbohydrate content affect the sinking rates of marine diatoms? *J. Phycol.* **32**, 360–365. (doi:10.1111/j.0022-3646.1996.00360.x)
41. Clapham DE. 1995 Calcium signaling. *Cell* **80**, 259–268. (doi:10.1016/0092-8674(95)90408-5)
42. Amato A *et al.* 2017 Marine diatoms change their gene expression profile when exposed to microscale turbulence under nutrient replete conditions. *Sci. Rep.* **7**, 3826. (doi:10.1038/s41598-017-03741-6)
43. Crocker JC, Grier DG. 1996 Methods of digital video microscopy for colloidal studies. *J. Colloid Interface Sci.* **179**, 298–310. (doi:10.1006/jcis.1996.0217)
44. Gargett AE. 1989 Ocean turbulence. *Annu. Rev. Fluid Mech.* **21**, 419–451. (doi:10.1146/annurev.fl.21.010189.002223)

45. Jiménez J. 1997 Oceaninc turbulence at millimeter scales. *Scientia Marina* **61**, 47–56.
46. Mitchell J, Yamazaki H, Seuront L, Wolk F, Li H. 2008 Phytoplankton patch patterns: seascape anatomy in a turbulent ocean. *J. Mar. Syst.* **69**, 247–253. (doi:10.1016/j.jmarsys.2006.01.019)
47. Legendre P, Fortin MJ. 1989 Spatial pattern and ecological analysis. *Vegetatio* **80**, 107–138. (doi:10.1007/BF00048036)
48. Polis GA, Anderson WB, Holt RD. 1997 Toward an integration of landscape and food web ecology: the dynamics of spatially subsidized food webs. *Annu. Rev. Ecol. Syst.* **28**, 289–316. (doi:10.1146/annurev.ecolsys.28.1.289)
49. Mackas DL, Denman KL, Abbott MR. 1985 Plankton patchiness: biology in the physical vernacular. *Bull. Mar. Sci.* **37**, 652–674.
50. Martin A. 2003 Phytoplankton patchiness: the role of lateral stirring and mixing. *Progr. Ocean.* **57**, 125. (doi:10.1016/S0079-6611(03)00085-5)
51. Visser AW, Kiørboe T. 2006 Plankton motility patterns and encounter rates. *Oecologia* **148**, 538–546. (doi:10.1007/s00442-006-0385-4)
52. Kiørboe T. 2008 *A mechanistic approach to plankton ecology*. Princeton, NJ: Princeton University Press.
53. Durham WM, Stocker R. 2012 Thin phytoplankton layers: characteristics, mechanisms, and consequences. *Annu. Rev. Mar. Sci.* **4**, 177–207. (doi:10.1146/annurev-marine-120710-100957)
54. Durham WM, Climent E, Barry M, De Lillo F, Boffetta G, Cencini M, Stocker R. 2013 Turbulence drives microscale patches of motile phytoplankton. *Nat. Commun.* **4**, 2148. (doi:10.1038/ncomms3148)
55. Arrieta J, Barreira A, Tuval I. 2015 Microscale patches of nonmotile phytoplankton. *Phys. Rev. Lett.* **114**, 128102. (doi:10.1103/PhysRevLett.114.128102)
56. Borgnino M, Arrieta J, Boffetta G, De Lillo F, Tuval I. 2019 Turbulence induces clustering and segregation of non-motile, buoyancy-regulating phytoplankton. *J. R. Soc. Interface* **16**, 20190324. (doi:10.1098/rsif.2019.0324)
57. Maxey MR, Riley JJ. 1983 Equation of motion for a small rigid sphere in a nonuniform flow. *Phys. Fluids* **26**, 883–889. (doi:10.1063/1.864230)
58. Cartwright J, Feudel U, Károlyi G, de Moura A, Piro O, Tél T. 2010 Dynamics of finite-size particles in chaotic fluid flows. In *Nonlinear dynamics and chaos: advances and perspectives. Understanding complex systems.* (ed. M Thiel, J Kurths, M Romano, G Károlyi, A Moura), pp. 51–87. Berlin, Heidelberg: Springer.
59. Taylor GI. 1923 LXXV. On the decay of vortices in a viscous fluid. *Lond. Edinburgh Dublin Phil. Mag. J. Sci.* **46**, 671–674. (doi:10.1080/14786442308634295)
60. Drazin P, Riley N, Society LM, Staff LMS 2006 *The Navier-Stokes equations: a classification of flows and exact solutions*. London Mathematical Society Lecture Note Series. Cambridge, UK: Cambridge University Press.
61. Frisch U. 1995 *Turbulence - the legacy of A.N. Kolmogorov*. Cambridge, UK: Cambridge University Press.
62. Crisanti A, Falcioni M, Provenzale A, Vulpiani A. 1990 Passive advection of particles denser than the surrounding fluid. *Phys. Lett. A* **150**, 79–84. (doi:10.1016/0375-9601(90)90253-K)
63. Cartwright JHE, Magnasco MO, Piro O, Tuval I. 2002 Bailout embeddings and neutrally buoyant particles in three-dimensional flows. *Phys. Rev. Lett.* **89**, 264501. (doi:10.1103/PhysRevLett.89.264501)
64. Maxey MR, Corrsin S. 1986 Gravitational settling of aerosol particles in randomly oriented cellular flow fields. *J. Atmos. Sci.* **43**, 1112–1134. (doi:10.1175/1520-0469(1986)043<1112:GSOAPI>2.0.CO;2)
65. Maxey MR. 1987 The motion of small spherical particles in a cellular flow field. *Phys. Fluids* **30**, 1915–1928. (doi:10.1063/1.866206)
66. Stommel H. 1949 Trajectories of small bodies sinking slowly through convection cells. *J. Mar. Res.* **8**, 24–29.
67. Calzavarini E, Cencini M, Lohse D, Toschi F. 2008 Quantifying turbulence-induced segregation of inertial particles. *Phys. Rev. Lett.* **101**, 084504. (doi:10.1103/PhysRevLett.101.084504)
68. Falkowski PG, Barber RT, Smetacek V. 1998 Biogeochemical controls and feedbacks on ocean primary production. *Science* **281**, 200–206. (doi:10.1126/science.281.5374.200)
69. Sengupta A, Carrara F, Stocker R. 2017 Phytoplankton can actively diversify their migration strategy in response to turbulent cues. *Nature* **543**, 555–558. (doi:10.1038/nature21415)